Turbulent energy transfer into zonal flows from the weak to the strong flow shear regime in the stellarator TJ-K

T. Ullmann,[1] B. Schmid,[1] P. Manz,[2] G.E.M. Tovar,[1] and M. Ramisch[1]
[1)] *Institute for Interfacial Process Engineering and Plasma Technology (IGVP), University of Stuttgart*[a)]
[2)] *Max Planck Institute for Plasma Physics Garching, Germany*[b)]

(Dated: 30 November 2020)

The transition from low to high confinement in fusion experiments is accompanied by a reduction of turbulence in the strong shear regime. This work investigates the influence of the background shearing rate on the energy transfer between turbulence and zonal flows, which can serve as a loss channel of kinetic energy, in the different shear regimes using the k-ε model. To this end, plasma biasing is used to control the flow shear which is categorized in terms of measured turbulent lifetime. The shearing rate scaling of Reynolds stress and zonal flow production is analyzed. A linear dependency of the Reynolds stress and a quadratic dependency of the energy transfer on the shearing rate is found. This is accompanied by a redistribution of the spectral power towards the zonal flow. The increase in relative zonal power is even higher beyond the transition to the strong shear regime.

I. INTRODUCTION

In magnetized fusion plasmas the transition from a low (L) to a high (H) confinement regime is accompanied by a reduction of the turbulence level and turbulent transport.[1] This reduction may be due to the transfer of energy from small scale turbulence to macroscopic turbulent structures, which are not associated with cross-field transport, known as turbulence generated zonal flows (ZF).[2] Indeed, first experimental results provided an indication that ZFs may trigger the fast LH-transition.[3–10] The transition to the H-mode is accompanied by a transition from a weak to a strong shear regime. A strong shear regime is present if the $E\times B$-shearing rate is larger than the growth rate of most unstable mode.[11] According to the k-ε model the energy transfer depends quadratically on the shearing rate. Since the kinetic energy in the turbulence is reduced in the strong shear regime, the question arises whether the energy transfer collapses with the transition, too. Further, this work deals with the question to what extent the background shear contributes to a redistribution of the spectral power in favor of the ZF.

In magnetically confined fusion plasmas, ZFs are associated with poloidally and toroidally homogeneous, as well as, radially localized plasma potential perturbations. Here, the plasma potential takes over the role of the stream function as compared to neutral fluids. In analogy to neutral fluids, macroscopic turbulence generated flows are driven by gradients in the turbulent Reynolds stress ($\partial_r\langle\tilde{v}_r\tilde{v}_\theta\rangle$). Finite Reynolds stress (RS) can be traced back to tilted vortex flow fields.[12] Thus equilibrium shear flows can principally affect the RS by tilting vortices which in turn can lead to a higher RS gradient and thus to an increase in ZF amplitudes. In particular, the RS is expected to increase linearly with the background shear when viewed in the picture of turbulent viscosity.[13] According to the k-ε model, the product of shear and RS is the production of kinetic energy of the mean flow, which implies a quadratic dependence of energy transfer into the ZF.[14] In addition, as energy is transferred from smaller to larger eddies, a substantial change in spectral power distribution across turbulent scales could be expected.[15]

How far this redistribution takes place in favour of ZFs in toroidal geometry is investigated experimentally at magnetically confined low-temperature plasmas in the stellarator TJ-K.[16] To this end, shear in the equilibrium plasma flow is imposed by externally controlling the stationary plasma potential profile through electrode biasing.[17] Electrode biasing can be used to trigger H-mode-like regimes, where the transition appears similar to the ones reported in from spontaneous L-H transitions reported in Ref.[5,8–10,18] Shearing rates as deduced from plasma potential measurements are opposed to experimental estimates of zonal averages of turbulent RS and potential fluctuations. A flux-surface aligned multiprobe setup with 128 probes is used to resolve fluctuations relevant for RS and ZF estimates.[12]

A key issue is to differentiate between the stationary equilibrium $E\times B$-flow and the self-generated ZF. While the plasma potential can be considered constant on the flux surface in TJ-K, the inhomogeneity of the confining magnetic field leads to a poloidal variation of the $E\times B$-background flow and corresponding shear. The k-ε model is adapted to the energy transfer between ZFs as poloidal mean flows and turbulence by applying a poloidal average as Reynolds average on the total velocity field consisting of the time-fluctuating and stationary velocities. Although the energy evolution of the mean flow does not depend on the time-independent component, the energy transfer term has a dependence on the stationary flow which is discussed in sec. II by a further decomposition in time. After a description of the experimental setup (sec. III) it is shown how the shearing rate is obtained in TJ-K and controlled with biasing. By comparison with mean growth rates from the elliptical model the different shear regimes are identified (sec. IV). In the next section the dependency of RS and production is investigated (sec. V). Finally, spectral analyses are used to investigate the redistribution of power as a function of energy transfer and shearing rate (sec. VI).

[a)] https://www.igvp.uni-stuttgart.de/pd
[b)] https://www.ipp.mpg.de/en

II. MODEL EQUATIONS

A model which describes the energy of the fluctuations and the mean flow is the k-ε model. Here the energy evolution of the mean flow is derived by multiplying the Reynolds averaged Navier-Stokes equation (RANS) by the mean flow velocity (U). By neglecting the dissipation term (ε), the k-ε model for the two-dimensional case, with x as radial and y as corresponding poloidal plane-coordinate, finally yields for the poloidal mean-flow energy ($\bar{E} = 0.5U_y^2$) [5,15,19]

$$\partial_t \bar{E} + \partial_x \bar{T} = R\partial_x U_y := \mathscr{P} \,, \tag{1}$$

with $\bar{T} = RU_y$ and $R = \langle \tilde{u}_x \tilde{u}_y \rangle$ the RS, with $\tilde{u}$ as the fluctuating part of the Reynolds decomposition. The Navier-Stokes equation is subtracted by the RANS and multiplied by the fluctuating velocity, so that after a further Reynolds average the fluctuating energy finally yields;[14]

$$\partial_t \tilde{E} + \partial_x \tilde{T} = -R\partial_x U_y := -\mathscr{P} \,, \tag{2}$$

with $\tilde{T} = 0.5\langle \tilde{u}_x \tilde{u}_y \tilde{u}_y \rangle_Y$, where $\langle \cdot \rangle_Y$ denotes a spatial, i.e. poloidal average. A comparison of the energy evolution of the mean flow (eq. (1)) with the one from the fluctuations (eq. (2)) shows the importance of the so-called production term

$$\mathscr{P} = R\partial_x U_y = \langle \tilde{u}_x \tilde{u}_y \rangle_Y \partial_x U_y \tag{3}$$

The production term connects the evolution of the mean flow with the one of the fluctuations. A positive production ($\mathscr{P} > 0$) can be physically interpreted as an energy transfer from the turbulence into the mean flow and therefore "produces" the mean flow. Respectively, turbulence is generated by the mean flow, if the production is negative ($\mathscr{P} < 0$). The direction of the energy transfer depends on whether the RS and the shear ($\partial_x U_y$) do have the same sign. If they do not, then the velocity field of the eddies counteracts the shear in the mean flow and energy is transferred from the mean flow into the turbulence. In the case of a positive production, the eddies are strained out by the shear flow towards larger structures, i.e. the mean flow itself.[20] This energy transfer from small to large scale structures is accompanied by the inverse cascade.[21] Furthermore, a positive correlation between the sheared mean flow and the RS implies a negative turbulent viscosity ν_T as theoretically proposed for two-dimensional systems ($R = -\nu_T \partial_x U_y$).[13]

The investigation of the influence of the time-independent shear on the turbulence requires to distinguish between a spatial $\langle \cdot \rangle_Y$ and a temporal average $\langle \cdot \rangle_T$ of the velocity, such that $\langle u \rangle_Y = \langle U + \tilde{u} \rangle_Y$ with $\langle \tilde{u} \rangle_Y = 0$ and $\langle V \rangle_T = \langle V + \tilde{v} \rangle_T$ with $\langle \tilde{v} \rangle_T = 0$. Here, for the Reynolds decomposition the spatial average is chosen, in order to examine the ZF component. In order to investigate the influence of the background shearing rate on the power in the ZF, eq. (1) is time-averaged. The time-derivative of the mean kinetic energy on the left-hand side of eq. (1) then reads

$$\frac{1}{2}\langle \partial_t U_y^2 \rangle_T = -i\omega \left\langle \langle \tilde{v}_y \rangle^2 \right\rangle_T \,. \tag{4}$$

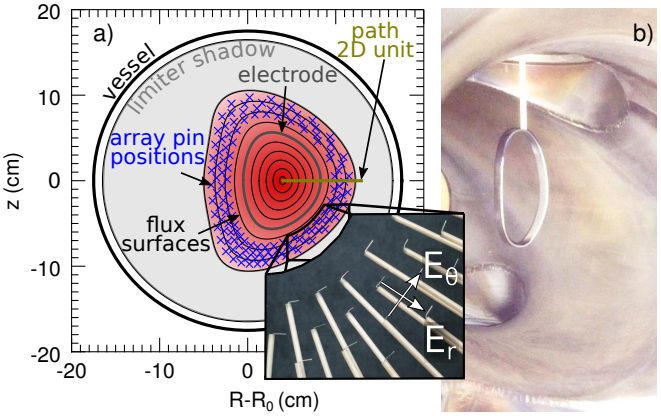

FIG. 1. a) Scheme of experimental setup showing the path of the movable emissive probe, the flux surface of the ring electrode (thick) and the projected pin positions of the array as crosses. The photo of the array indicates the direction of the radial and poloidal electric field fluctuations, needed to obtain the RS. b) A photo of the ring electrode placed at a top-port, where the flux surfaces are elliptical.

By considering the $E\times B$-velocity this expression is proportional to the power in the zonal potential and does not depend on the time-independent velocity components

$$\frac{1}{2}\langle \partial_t U_y^2 \rangle_T \propto \langle \phi_{ZF}^2 \rangle_T \,. \tag{5}$$

Now the influence of the background shearing rate on the energy transfer will be investigated. The spatial fluctuations of the RS are related to temporal fluctuations as

$$\begin{aligned} \tilde{u}_x \tilde{u}_y &= (V_x + \tilde{v}_x)(V_y + \tilde{v}_y) - (V_x + \tilde{v}_x)\langle V_y + \tilde{v}_y \rangle_Y \\ &= \tilde{v}_x V_y + \tilde{v}_x \tilde{v}_y - [\, \tilde{v}_x \langle V_y \rangle_Y \, + \tilde{v}_x \langle \tilde{v}_y \rangle_Y \,] \,, \end{aligned} \tag{6}$$

such that the resulting temporally averaged production consists of mixed contributions

$$\begin{aligned} \langle \mathscr{P} \rangle_T = &\left\langle \, \langle \tilde{v}_x V_y \rangle_Y \, \partial_x \langle \tilde{v}_y \rangle_Y \, \right\rangle_T + \langle \tilde{v}_x \tilde{v}_y \rangle_{Y,T} \partial_x \langle V_y \rangle_Y \\ &+ \left\langle \, \langle \tilde{v}_x \tilde{v}_y \rangle_Y \, \partial_x \langle \tilde{v}_y \rangle_Y \, \right\rangle_T \,. \end{aligned} \tag{7}$$

The bracket $\langle \cdot \rangle_{Y,T}$ denotes a poloidal as well as temporal average. Only the second part shows a dependence on the background shear flow ($\partial_x \langle V_y \rangle_Y$) while the other contributions only lead to an offset of the mean production. As the RS itself can be expressed by the negative product of the turbulent viscosity and the shearing rate, the second term in eq. 7 results in a quadratic dependency on the temporally and poloidally averaged shearing rate.[14]

The model suggests that the background shear leads to an energy transfer from the turbulence to the mean flow, i.e. the ZF. Disregarding loss channels for ZF energy. the relative ration of the ZF to the total spectral power may be expected to increase with the shearing rate.

III. EXPERIMENTAL SETUP

The low-temperature plasmas in the stellarator TJ-K ($T_e \leq 20\,\mathrm{eV}$, $T_i \approx 1\,\mathrm{eV}$)[22] allow to place a ring-shaped, flux-

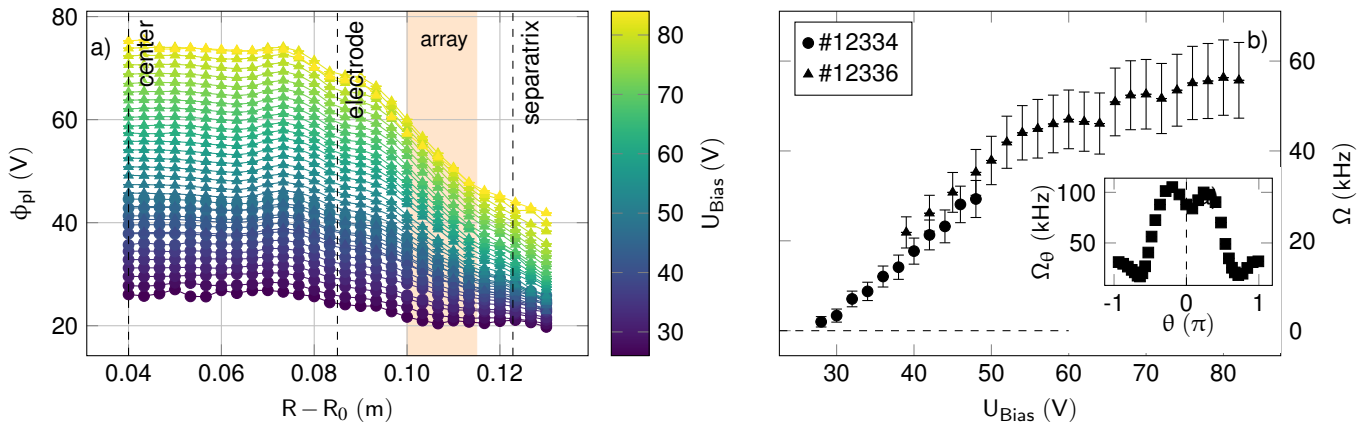

FIG. 2. a) Radial profile of the plasma potential measured by a radially movable emissive probe. Important radial positions are marked as dashed vertical lines. b) The inlay shows an exemplary poloidal profile of the shearing rate at a high bias case ($U_{\mathrm{Bias}} = 72\,\mathrm{V}$). The poloidally averaged shearing rate is plotted against the bias voltage of the electrode for two different shots (different symbols). The shearing rate increases monotonously with the bias voltage.

surface-aligned electrode within the confinement region (see fig. 1-b)). Due to the currents drawn by the electrode, a radial electric field is formed, whose $E \times B$ rotation balances corresponding the friction forces, associated with magnetic pumping, against forces through radial return currents neutralising the charge-loss through the electrode.[17,23] This way, the background $E \times B$ rotation is controlled through the current drawn by the electrode.[24] Zonal flows have been studied in TJ-K in detail without biasing.[12,20,25,26] With biasing enhanced zonal flow activity have been found.[27,28]

In the experiment TJ-K, the profile of the plasma potential is measured by a radially moving emissive probe as indicated in fig. 1-a) allowing to calculate the $E \times B$-velocity and shearing rate. Further, equilibrium parameters as the electron temperature and the density are obtained from an additional, swept Langmuir probe on the same carrier as the emissive probe. The floating potential is measured by 128 Langmuir probes distributed on four consecutive flux surfaces (fig. 1-a) as crosses) acquiring simultaneously 2^{19} samples per probe at 1 MHz sampling rate.[12] The radial and poloidal velocity fluctuations, needed for the RS calculation, are derived from the fluctuating electric fields in poloidal and radial direction as the inlay shows ($\tilde{v}_r \propto \tilde{E}_\theta$ and $\tilde{v}_\theta \propto -\tilde{E}_r$). The electric fields are calculated from the difference quotients of the fluctuations in the floating potential ($\tilde{E}_r = \left[\tilde{\phi}_{\mathrm{fl}}(r_i) - \tilde{\phi}_{\mathrm{fl}}(r_j)\right] / \left[r_j - r_i\right]$ and $\tilde{E}_\theta = \left[\tilde{\phi}_{\mathrm{fl}}(\theta_i) - \tilde{\phi}_{\mathrm{fl}}(\theta_j)\right] / \left[r\theta_j - r\theta_i\right]$).

Temperature fluctuations are negligible which allows to take advantage of the approximation $\tilde{\phi}_{\mathrm{fl}} \approx \tilde{\phi}_{\mathrm{pl}}$.[29] The array allows to calculate kf-spectra of the band-passed potential fluctuations (3 kHz − 400 kHz) which are used to obtain the power in the ZF component ($k = 0$ at 3 kHz − 8 kHz) and the power in the remaining turbulent spectrum.[26]

The hydrogen plasma is heated by a 2.45 GHz microwave at a power of $P_{2.45} = 2.5\,\mathrm{kW}$. The neutral gas working pressure is $p_0 = 9\,\mathrm{mPa}$. The bias voltage of the electrode - as control parameter - is increased stepwise ($\Delta U = 2\,\mathrm{V}$) within two discharges (#12334, #12336). At each step the equilibrium and fluctuations of the plasma are measured by the emissive/swept Langmuir probe and by the array, too.

IV. CONTROLLING THE SHEAR

The development of the plasma potential profiles with changing bias voltage is shown in fig. 2-a). The radial profile covers the full range from the plasma center to outside the last closed flux surface. The plasma potential raises with increasing bias voltage. Further, the gradient of the plasma potential steepens with higher bias voltages in the region between electrode and separatrix, thus changing the poloidal $E \times B$-velocity. In this region the probe array is positioned. A strong effect of the flow shear on the tilt of turbulent structures is supposed to be detected by the array.

In order to compare the shearing rate with the two-dimensional RS measurements, the equilibrium potential is mapped on the flux surface since the plasma potential is a flux quantity. The $E \times B$ velocity is calculated, incorporating the metrics of the magnetic field geometry (cf. inlay fig. 2-b)). For a comparison of the shearing rate with the RS, the shearing rate is defined by the radial change in the angular velocity as $\Omega = (2\pi)^{-1} \langle r \partial_r (v_{E\times B}/r) \rangle_\theta$. The shearing rate is poloidally averaged ($\langle \cdot \rangle_\theta$). Fig. 2-b), shows how the shearing rate can be controlled by the bias voltage. With increasing bias voltage, the shearing rate increases, too.

In a next step, two different shear regimes are identified. A low shear regime is determined by a shearing rate lower than the inverse mean growth time of turbulent structures (τ_g) and the strong shear regime by shearing rates exceeding the inverse growth time.[31] A transition threshold is defined as $\zeta = \Omega \tau_g^{-1} = 1$. A value $\zeta < 1$ implies a weak shear regime and a value $\zeta > 1$ a strong shear regime. In the latter case, the shear tilts the turbulent structures faster than they can evolve and turbulence suppression is supposed to become effective.

In order to experimentally obtain the inverse mean growth time (τ_g) of the evolving turbulent structures, the cross-correlation of the fluctuations in poloidal direction (θ) and in

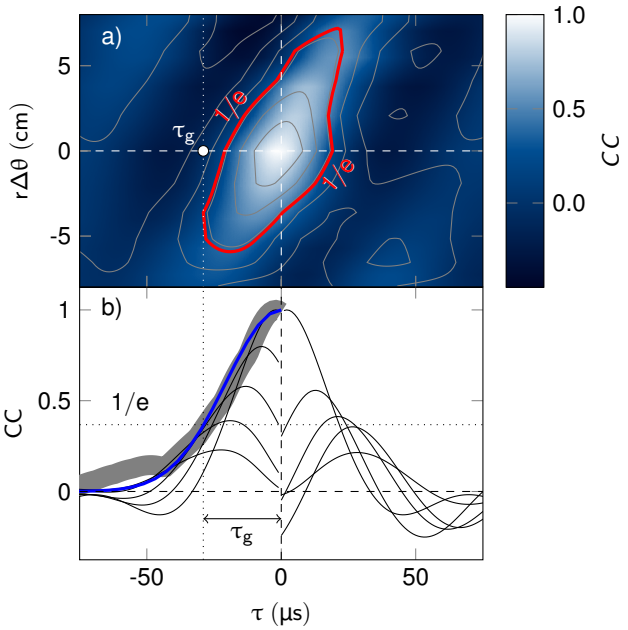

FIG. 3. a) The cross-correlation function in two dimensions with the poloidal shift Δy on the ordinate and the time shift τ on the abscissa. The red contour line marks the e^{-1}-level, which has roughly the shape of an ellipse. b) The growth time (τ_g) is obtained from the width of a Gaussian fit to the envelope of the different cross-correlations over the negative time shift τ.

time can be estimated by the elliptical model

$$CC(\tau, r\Delta\theta) = \exp\left[-\left(\frac{\tau^2}{\tau_c^2} + \frac{(r\Delta\theta - V_\theta\tau)^2}{L_\theta^2}\right)\right], \quad (8)$$

where τ is the time-shift and $r\Delta\theta$ the spatial, poloidal shift and V_θ the background velocity. The contours in the τ, $r\Delta\theta$-space show the ellipses. Typical time (τ_c) and length (L_θ) scales describe the correlation time and poloidal size of the structures. In contrast to the "frozen turbulence" theorem of the Taylor-hypothesis, the model takes an intrinsic, average life-time of turbulent structures into account. Since their growth and decay do not necessarily show the same behavior, it is useful to split the cross-correlation in a part for negative and positive time-shifts. This enables to differentiate between growth time $\tau_c \to \tau_g$ and decay/decorrelation time $\tau_c \to \tau_d$. The correlation times $\tau_{g,d}$ are not obtained from the $1/e$ folding time at $r\Delta\theta = 0$, but from the minimum/maximum value of the time shift τ from the $CC(\tau, r\Delta\theta) = 1/e$ contour ellipse.[32] Similar models have been used in Ref.[33,34].

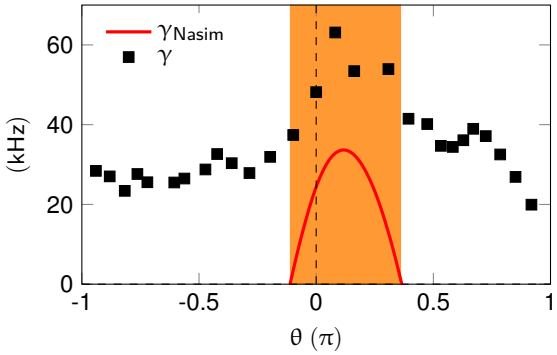

FIG. 4. The poloidal profile of the inverse growth times ($\gamma = \tau_g^{-1}$) as squares agree qualitatively well with the calculated maximum growth rates (line) incorporating the magnetic field geometry according to Nasim.[30] The local maximum of the growth rate is found in a region where the calculated growth rate exhibits a postive maximum (red area), too.

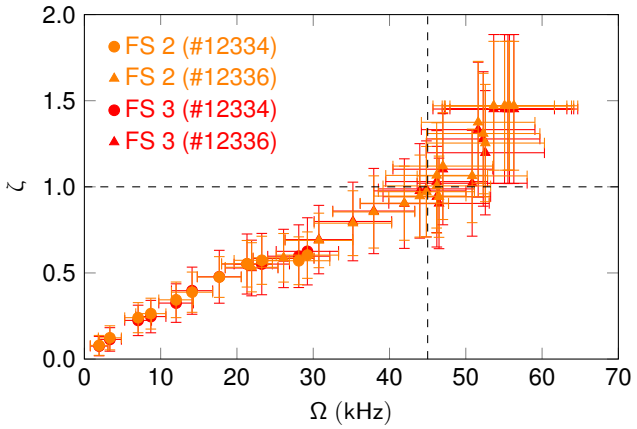

FIG. 5. The ratio ($\zeta = \Omega\tau_g^{-1}$) plotted against the shearing rate. The range of $\Omega = 0\,\mathrm{kHz} - 45\,\mathrm{kHz}$ denotes the weak shear regime, whereas the range higher than $\Omega > 45\,\mathrm{kHz}$ the strong shear regime.

The proposed elliptical character of the CC in TJ-K can be seen from fig. 3-a) for one exemplary reference probe of the array. Fig. 3-b) shows the cross-correlations for different poloidal positions ($r\Delta\theta$) over the time-lag (τ). In order to obtain the growth time τ_g, the envelope of all cross-correlations of negative time shifts ($\tau \leq 0$) is fitted by a Gaussian ($CC(\tau) = \exp\left[-(\tau/\tau_g)^2\right]$). The average growth time τ_g is the minimal possible time-shift that defines the edge of the $1/e$-ellipse for negative times (white dot in fig. 3-a)). The fit is done for every probe pin of the array ($\tau_g(\theta)$). The inverse growth time can be interpreted as an effective, average growth rate. The poloidal profile of the growth rate is shown in fig. 4 for a low shear case ($\Omega \approx 0$). It exhibits a maximum at $\theta \approx 0.1\pi$ which qualitatively agrees well with the maximum linear growth rate calculated according to Nasim[30] incorporating the magnetic field geometry. For comparison with the shearing rate the growth rate is finally averaged over the poloidal angle.

In fig. 5, the ratio of the poloidally averaged quantities $\zeta = \Omega\tau_g^{-1}$ is shown in dependence of the shearing rate. Values of the ratio below one, marked by a horizontal line, refer to the low shear regime and value above to the strong shear regime. For the presented hydrogen discharges it is found that the transition takes place at a shearing rate of $\Omega \approx 45\,\mathrm{kHz}$ (vertical line).

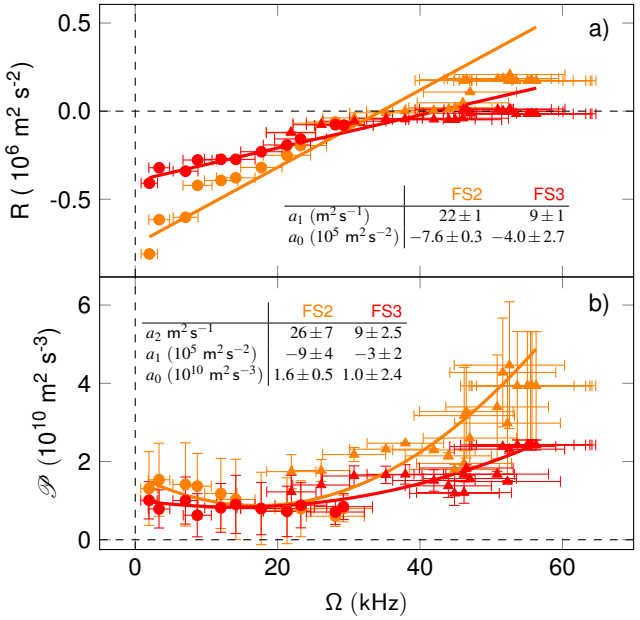

FIG. 6. a) The poloidally and temporally averaged Reynolds stress for two different flux surfaces (orange, inner and red, outer) plotted against the shearing rate. With increasing shearing rate the Reynolds stress increases roughly linearly and has a zero-crossing at around $\Omega \approx 40\,\mathrm{kHz}$. b) The production term calculated according to eq. (7) plotted against the shearing rate. Positive values indicate that the energy is transferred from the turbulence into the mean-flow (i.e. zonal flow). For higher shearing rates the energy transfer into the mean flow takes increases, too.

V. INFLUENCE OF THE SHEAR ON THE REYNOLDS STRESS AND THE ZONAL FLOW PRODUCTION

The background shear is supposed to change the tilt of the turbulent structures resulting in a non-vanishing RS as previous simulations suggest.[35] The local, time-averaged RS is expected to depend linear on the $E\times B$-shearing rate

$$R_{\mathrm{loc}}(\theta) = [\, -\Delta\theta_{\mathrm{d}}\hat{s} + \Omega_{\mathrm{loc}}(\theta)\tau_L(\theta)\,]\ \langle\tilde{v}_r^2\rangle_T\ , \qquad (9)$$

where $\Delta\theta_{\mathrm{d}}$ is the poloidal distance to the ballooning peaking position, $\hat{s}$ the global magnetic shear, Ω_{loc} the local $E\times B$-shearing rate and $\tau_L = \tau_g + \tau_d$ the life-time of the turbulent structures. For the flux surface averaged RS in the confinement region, simulations show that the magnetic shear is negligible because of its symmetry[19] and the value of the global shear in TJ-K is low at the array position ($\hat{s} \approx -0.05$).

In the experiment TJ-K, the RS ($\langle\tilde{v}_r\tilde{v}_\theta\rangle$) is poloidally available from the array (see. III).[12] The RS is averaged both temporally and poloidally, as was previously applied in the case of the background shearing rate. Both are plotted against the shearing rate in fig. 6-a). The figure shows a roughly linear dependence of the RS on the shearing rate, as theoretically expected from eq. (9). The fit parameters are shown as inlay and show a slightly different behavior depending on the radial position. The positive correlation between the background shearing rate and the RS confirms the concept of a negative turbulent viscosity $R \approx -\nu_T\Omega + a_0$ with the expected offset at zero shear. Since the life-time, the power in the radial velocity fluctuations and the shearing rate can vary poloidally the lifetime or radial velocity fluctuations may weight the shearing rate differently and the RS is not necessarily zero if the mean shearing rate is zero ($R(\Omega = 0) \approx \langle\Omega_{\mathrm{loc}}\tau_L\tilde{v}_r^2\rangle_T\rangle_\theta \neq 0$).

As defined in sec. II, an energy transfer from the turbulence into the mean flow takes place, if the production term is positive. The production term as derived in eq. (7) is calculated from the experimental data (sec. III) and is plotted against the shearing rate in fig. 6-b). All values are positive, which implies an energy transfer from the turbulence into the poloidal mean flow, as it is expected from the inverse cascade in two-dimensional turbulent systems. The production term depends roughly quadratically on the shear but the coefficients again depend on the radial position. The quadratic behavior is expected from eq. 7, where the second term consists of the background RS and the background shearing rate ($R(\partial_x V)^2$). For both dependencies, the RS and the production term no significant change is found when entering the strong shear regime.

VI. REDISTRIBUTION OF POWER

As a consequence of the higher production at higher shear, a redistribution of the energy towards the ZF is expected. For verification, the frequency integrated k-spectrum of the potential fluctuations in fig. 7 shows the power distribution for selected shearing rates. Here, the wavenumber is normalized by $\rho_s = \sqrt{m_i T_e}/(eB_0)$, where T_e is obtained from the swept Langmuir probe, and the upper axis respectively shows the poloidal mode number (m). Besides the $m = k\rho_s = 0$ mode, which is related to the ZF, an $m = -4$ mode shows up which could be related to the rotational transform ($\iota\approx 0.25$) for TJ-Ks magnetic field which could stimulate the $m = -4$ mode as most unstable eigen mode[30] in the system. For the increasing shearing rate, the power in the broadband turbulence decreases. This drop is stronger than the changes in the ZF power. Therefore, this

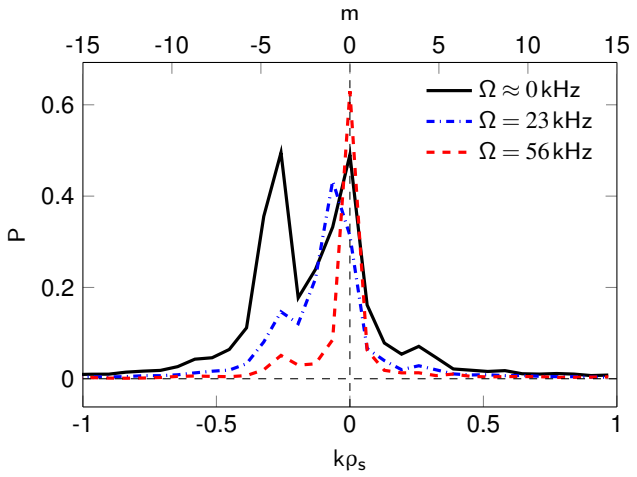

FIG. 7. Frequency integrated wavenumber power-spectra for different shearing rates. The local maximum at $m = -4$ may be related to the rotational transform ($\iota\approx 0.25$) for TJ-Ks magnetic field. With increasing shear, the $m = 0$ mode gains more power relative to the other modes, i.e. the power is redistributed.

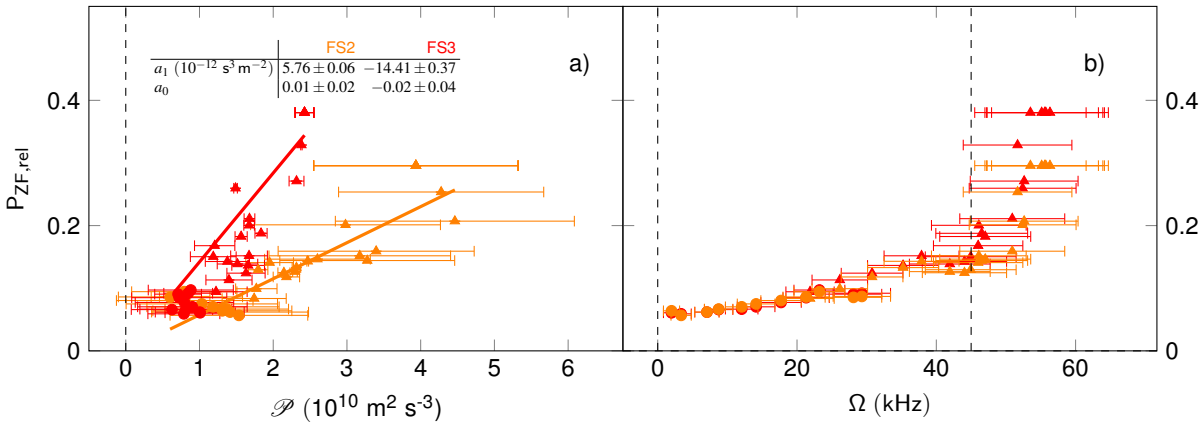

FIG. 8. a) The linear dependency between production and relative ZF power, which is the $m = 0$ power normalized on the total power. It describes a redistribution of the power as described by the k-ε model. b) With increasing shearing rate the relative ZF power increases and reaches its highest level in the strong shear regime. This implies that increasing the background shear leads to an enhanced redistribution of the energy towards the ZF.

qualitatively describes a redistribution of the spectral power.

In order to quantify the redistribution, the ZF mode is filtered in the frequency-band 3 kHz-8 kHz and integrated. Further the ZF power is normalized to the power of the total kf-spectrum as done in a previous study.[26] This relative ZF power is plotted against the production term in fig. 8-a). The roughly linear behavior indicates that indeed an increase in the production takes place simultaneously with an increase of the relative ZF power. This verifies the power redistribution towards the ZF.

As mentioned before (sec. II), the production term for a two-dimensional turbulent system can be reduced to a shearing rate dependence. Further, the redistribution of power is traced back to the change in the shearing rate, too. As can be seen in fig. 8-b), the relative ZF power increases with the shearing rate. At a shearing rate of around 45 kHz (vertical line) the relative ZF power increases even more strongly. As shown in the classification of the shear (fig. 5), the system enters the strong shear regime at this shearing rate.

VII. SUMMARY AND CONCLUSIONS

The influence of the background $E\times B$-shearing rate on the redistribution of energy is experimentally studied for hydrogen discharges in the stellarator experiment TJ-K under externally controlled shear, which is achieved by electrode biasing. A low shear regime from $\Omega = 0\,\mathrm{kHz} - 45\,\mathrm{kHz}$ and a strong shear regime higher than $\Omega > 45\,\mathrm{kHz}$ are identified.

Following the k-ε model, the energy transfer, i.e. the production term, between the poloidal mean flow and the turbulence can be described by the product of the Reynolds stress and the shearing rate. In two-dimensional turbulence, as the one in the stellarator TJ-K, the Reynolds stress is supposed to be positive and to depend linearly on the shearing rate resulting in a quadratic dependency of the production on the flow shear. Both dependencies are confirmed by the experimental data justifying the RS approximation in terms of a negative viscosity.

The redistribution of the energy is qualitatively shown by k-spectra for selected shearing rates. It already indicates a different behavior of the zonal flow component compared to the broadband turbulence, which is reduced in the strong shear regime. For a quantitative study the relative zonal flow power normalized to the total power of the kf-spectrum is analyzed with respect to the production and the shearing rate. A roughly linear dependency of the relative zonal flow power on the energy transfer indicates that indeed the redistribution of the power can be inferred from the production term. In the strong shear regime, the relative zonal flow power increases with higher shearing rates and exhibits an even stronger increase. The increasing shearing rate appears to entail a change in the Reynolds stress and consequently of the production term which describes an energy transfer towards the zonal flow.

The results show that indeed the background shear is able to enhance the energy transfer from the broadband turbulence to the zonal flow. Recent investigations of the I-phase in ASDEX-Upgrade do not reveal any significant contribution of turbulence driven zonal flows to the mean flow.[36,37] It must be stressed that the present work focusses on the energetic zonal flow drive rather than damping, which co-determines final zonal flow activity. For high-temperature plasmas as in ASDEX-Upgrade and JFT-2M[38], zonal flows could be subject to, e.g., ion-viscous damping, which is practically absent in TJ-K plasmas because of low ion temperatures.[22] Regardless of the detailed effects of zonal flow damping - which is left for future studies - the present work clearly shows that the power redistribution occurs as a more effective loss channel of turbulence energy when background shear is active.

[1]Wagner, The European Physical Journal H **43**, 523 (2018).
[2]Diamond, S.-I. Itoh, K. Itoh, and T. S. Hahm, Plasma Physics and Controlled Fusion **47**, R35 (2005).
[3]Conway, C. Angioni, F. Ryter, P. Sauter, and J. Vicente, Physical Review Letters **106**, 065001 (2011).
[4]Xu et al., Physical Review Letters **107**, 055003 (2011).
[5]Manz et al., Physics of Plasmas **19**, 072311 (2012).
[6]L. Schmitz et al., Physical Review Letters **108**, 155002 (2012).
[7]M. Xu et al., Physical Review Letters **108**, 245001 (2012).
[8]Tynan et al., Nuclear Fusion **53**, 073053 (2013).

[9]Yan et al., Physical Review Letters **112**, 125002 (2014).
[10]Cziegler et al., Nuclear Fusion **55**, 083007 (2015).
[11]Burrell, Physics of Plasmas **4**, 1499 (1997).
[12]Schmid, P. Manz, M. Ramisch, and U. Stroth, New Journal of Physics **19**, 055003 (2017).
[13]Gama, M. Vergassola, and U. Frisch, Negative isotropic eddy viscosity: A common phenomenon in two dimensions, in *Navier—Stokes Equations and Related Nonlinear Problems*, edited by A. Sequeira, pages 351–355, Springer US, Boston, MA, 1995.
[14]Pope, *Turbulent flows*, Cambridge University Press, Cambridge ; New York, 2000.
[15]Schmitz, Nuclear Fusion **57**, 025003 (2017).
[16]Krause et al., Review of Scientific Instruments **73**, 3474 (2002).
[17]Taylor et al., Physical Review Letters **63**, 2365 (1989).
[18]Shesterikov et al., Physical Review Letters **111**, 055006 (2013).
[19]Manz et al., Physics of Plasmas **25**, 072508 (2018).
[20]Manz, M. Ramisch, and U. Stroth, Physical Review Letters **103**, 165004 (2009).
[21]Kraichnan, Physics of Fluids **10**, 1417 (1967).
[22]Enge, G. Birkenmeier, P. Manz, M. Ramisch, and U. Stroth, Physical Review Letters **105**, 175004 (2010).
[23]Weynant, Taylor, Vandenplas, Durodie, and Schweer, 17th EPS Conference on Controlled Fusion and Plasma Heating **14**, 287 (1990).
[24]Ramisch, F. Greiner, N. Mahdizadeh, K. Rahbarnia, and U. Stroth, Plasma Physics and Controlled Fusion **49**, 777 (2007).
[25]Birkenmeier, M. Ramisch, B. Schmid, and U. Stroth, Physical Review Letters **110**, 145004 (2013).
[26]Schmid, P. Manz, M. Ramisch, and U. Stroth, Physical Review Letters **118**, 55001 (2017).
[27]Manz, M. Ramisch, and U. Stroth, Physics of Plasmas **16**, 042309 (2009).
[28]Manz, M. Ramisch, and U. Stroth, Physical Review E **82** (2010).
[29]Mahdizadeh et al., Plasma Physics and Controlled Fusion **47**, 569 (2005).
[30]Nasim, T. Rafiq, and M. Persson, Plasma Physics and Controlled Fusion **46**, 193 (2004).
[31]Terry, Reviews of Modern Physics **72**, 109 (2000).
[32]Zhao and G.-W. He, Physical Review E **79** (2009).
[33]Pinzón et al., Plasma Physics and Controlled Fusion **61**, 105009 (2019).
[34]Prisiazhniuk et al., Plasma Physics and Controlled Fusion **59**, 025013 (2017).
[35]Fedorczak, P. Diamond, G. Tynan, and P. Manz, Nuclear Fusion **52**, 103013 (2012).
[36]Birkenmeier et al., Nuclear Fusion **56**, 086009 (2016).
[37]Cavedon et al., Nuclear Fusion **57**, 014002 (2017).
[38]Kobayashi et al., Physical Review Letters **111**, 035002 (2013).